

One-dimensional quasi-static continuum model of muscle contraction as a distributed control system

By Michael Aigner AND Jean Heegaard

1. Motivation and objectives

Human muscles provide the mechanical energy necessary to set the body in motion. Some muscles, such as those in the lower limbs, provide large forces required to walk or run while others, like those around the wrist, have the dexterity needed to perform complex tasks. Understanding how these muscles function is an integral component of comprehending skeletal motion. Models and simulations of muscles are used not only to analyze human locomotion, but also to design robotic devices or to treat orthopaedic abnormalities.

1.1 Background

Skeletal muscles consist of a dense three-dimensional array of sensors and actuators that constitute a complex distributed control system. The schematic in Fig. 1 elucidates the major components of this important system. Long and thick myosin fibers packed together into a matrix form the substance of the muscle. Each of these fibers is controlled, on a microscopic scale, by neural stimuli from the central nervous system. Through active control by the brain, each muscle generates a desired force output which, coordinated with the forces of other muscles, performs a specific task.

Despite the apparent complexity, most authors in the literature only consider one of two simplified models. The first, pioneered by A. V. Hill (1938), assumes a muscle to be a combination of linear springs and a nonlinear contractile element. The second approach, pioneered by A. F. Huxley (1957), views the muscle at the microscopic level by considering the physical and chemical interactions in one muscular unit called a sarcomere. Current muscle models are commonly limited by the following two limitations. First, most authors assume that a muscle is inherently one-dimensional, although physical intuition casts doubt on the validity of such a hypothesis. Second, yet equally profound, is the lack of consideration for the distributed nature of the neural control network (Zajac & Winters, 1990).

The long-term goal of this research is to develop a full three-dimensional continuum model with distributed control to accurately understand the complexity and dexterity of human muscles. As a basis for future work, the specific objective of the present report is to describe a one-dimensional muscle model based on a quasi-static nonlinear constitutive law. A distributed control field is introduced, but, at this preliminary stage, it is specified *a priori* rather than being the unknown field variable.

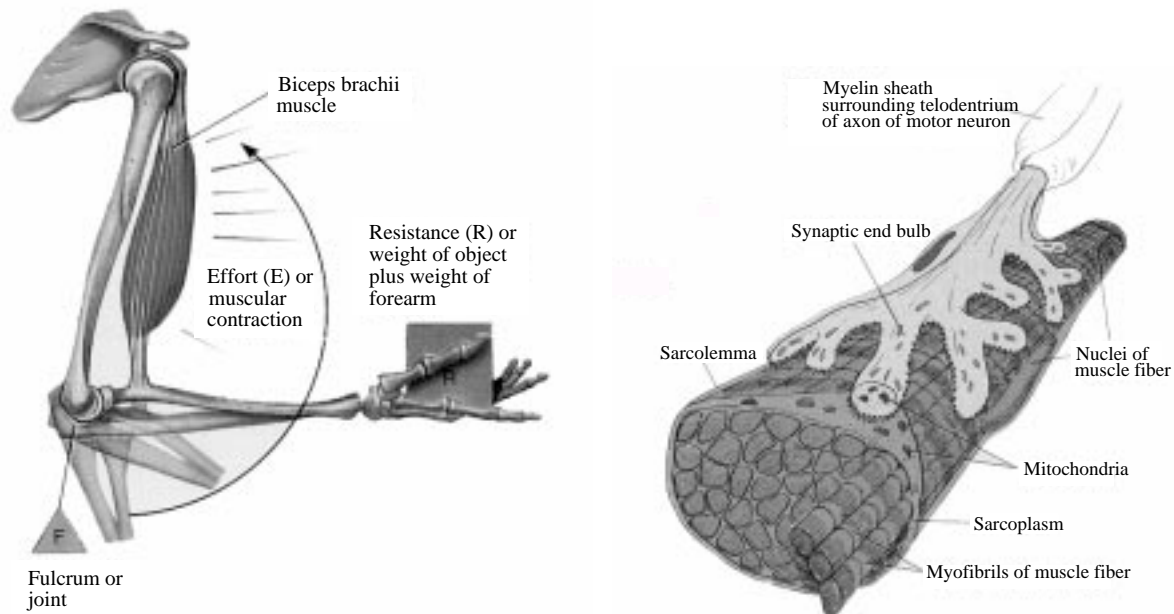


FIGURE 1. As a person lifts an object in their hand, the biceps muscle flexes to produce a resultant moment around the elbow. Zooming in on a microscopic level distinguishes the structure of the myosin fibers and the attached neural network.

1.2 Rheological model

We first consider a simple one-dimensional rheological muscle model for a sarcomere, as introduced by Huxley (1957). A sarcomere, depicted in Fig. 2a, consists of four physical components: thick myosin fibers, thin actin filaments, cross-bridges which link the actin to the myosin, and an external matrix to hold the muscle together. Although the myosin fibers provide the passive strength of the muscle, the active control from the central nervous system occurs in the cross-bridges. The level of neural activation in the muscle depends on the number of cross-bridges which attach to pull the myosin and actin fibers together to cause a contraction. This is why the model devised by Huxley is often referred to in the literature as the cross-bridge theory (Zahalak, 1990).

The model of the sarcomere can be understood by considering two scenarios. First, suppose the active components are completely inactive, meaning that none of the cross-bridges are attached. As the sarcomere is subjected to an outside load, only the external matrix prevents it from falling apart. Alternatively, when the central nervous system provides a stimulus, the cross-bridges are active, causing them to contract. Consequently, both the elastic myosin fibers and actin filaments become stretched. In addition, as the myosin fibers are pulled together by the cross-bridges, the elastic matrix contracts locally around the sarcomere.

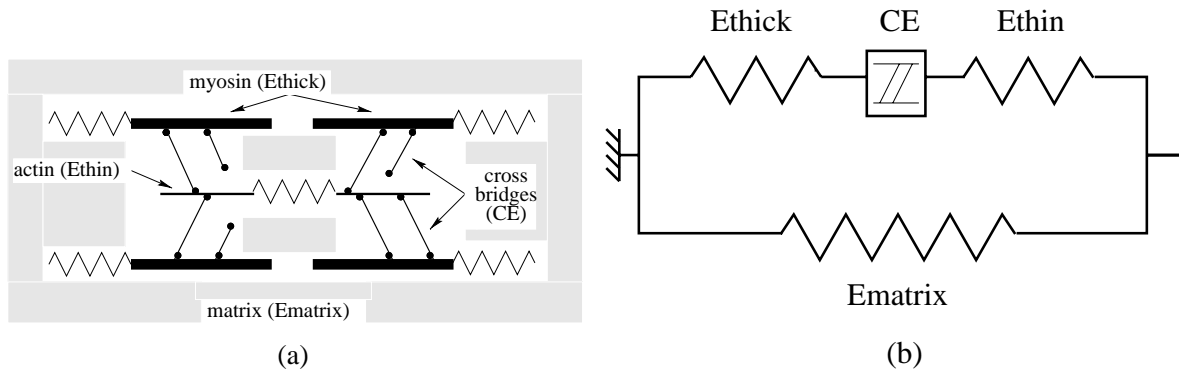


FIGURE 2. The physical model of the sarcomere (a) pioneered by Huxley depicts the cross-bridges which link the thick myosin fibers to thinner actin filaments. Each fiber has an intrinsic elasticity. This gives rise to a one-dimensional rheological model (b) with linear springs and a nonlinear contractile element (CE).

From these observations, the one-dimensional rheological model of Fig. 2b simulates the mechanics of the sarcomere. The behavior of the cross-bridges is represented by a nonlinear contractile element (CE). This component generates a force which depends on the sarcomere length, contractile velocity, and level of neural activation. The myosin and actin fibers connect in series with the cross-bridges. Since these are inherently passive elastic structures, they are depicted by linear springs. The myosin fibers (E_{thick}) are significantly thicker than the actin filaments (E_{thin}) meaning that the lumped stiffness is approximated by the stiffness of the myosin alone. Finally, the matrix (E_{matrix}) lies in parallel with the rest of the sarcomere, holding the entire system together. This parallel spring usually has a comparatively small stiffness, except for large strains (Winters, 1990). In order to model the damping of the muscle, viscous elements (dashpots) may be placed in parallel with each of the springs.

Consider again the two hypothetical scenarios above. In the case of no activation, the contractile element generates zero force so that both the thick and thin passive springs remain unstretched. Hence, all of the elastic characteristics of the muscle are contained in the matrix. Whenever the cross-bridges are active the contractile element generates a force. This same force is felt by both the myosin and the actin, causing both to stretch in accordance with Hooke's Law. The matrix, having only a small stiffness in the physiological range, is neglected when the muscle is active (Winters, 1990).

This one-dimensional rheological model is similar to the one devised by Hill (1938). However, while Hill's model is primarily used to represent the behavior of an entire muscle, our model is designed to capture the local behavior of the muscle in a continuum mechanics framework. By depicting the muscle as a series of these rheological models, each representing a single sarcomere, we seek to obtain a more accurate analysis of the effects of variations in muscle properties and activation. We therefore view the muscle as a continuum of sarcomeres excited by a *distributed* field of neural activation.

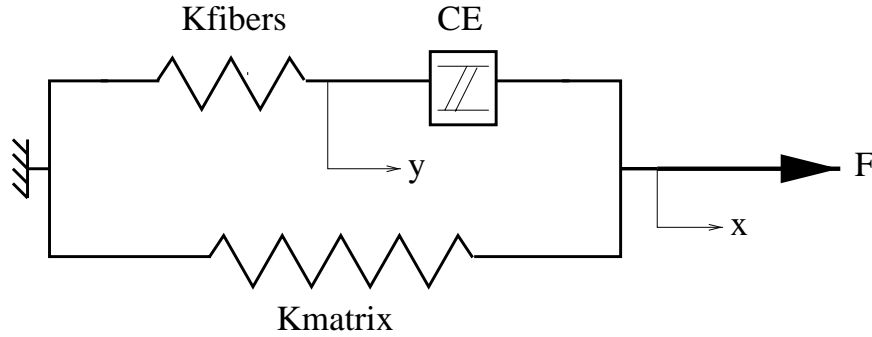


FIGURE 3. A simplified rheological model is used to derive the constitutive relationship.

2. Accomplishments

In order to implement a one-dimensional muscle model, we first derived a constitutive relationship using the rheological model in Fig. 3. We then used a simple model problem to formulate a weak form and expressed the solution of the resulting PDE using the Galerkin finite element method. The resulting nonlinear equations were solved using an exact Newton-Raphson linearization. Our results illustrate the relationship between displacement, stress, and activation along the length of the muscle.

2.1 Constitutive model

The constitutive model requires only a mathematical analysis of the rheological model of Fig. 3. The thick and thin springs have been lumped into one spring with constant K_{fibers} . We denote the matrix spring constant with K_{matrix} . In the present model problem, we assumed the left end to be fixed and denoted the displacement of the right end by x . Let y be the displacement of the spring representing the fibers. The displacement of the contractile element is then simply given by $x - y$.

We next establish the mathematical relationship governing the contractile element force generation. In this model, we approximate the force-length property of the muscle by a parabola in $x - y$ and neglect all dependence on velocity

$$F_{ce} = \frac{4}{l_o^2} F_{max} \alpha \left[(x - y) - \left(\frac{l_o}{2} \right) \right]^2 \quad (1)$$

The physical parameters are the nominal length l_o of the contractile element, the maximum isometric force F_{max} it can generate, and the activation α . Figure 4 illustrates this relationship, with each curve representing a different level of activation. A future analysis will also include a force-velocity relationship.

The problem is to determine the stress σ in the sarcomere given the displacement x and activation α . This is equivalent to finding the force F generated at the right end since $F = \sigma/A$, where A is the cross-sectional area of the sarcomere. The rheological model of Fig. 3 implies the following force relationship

$$F = F_{top} + F_{bottom} \quad (2)$$

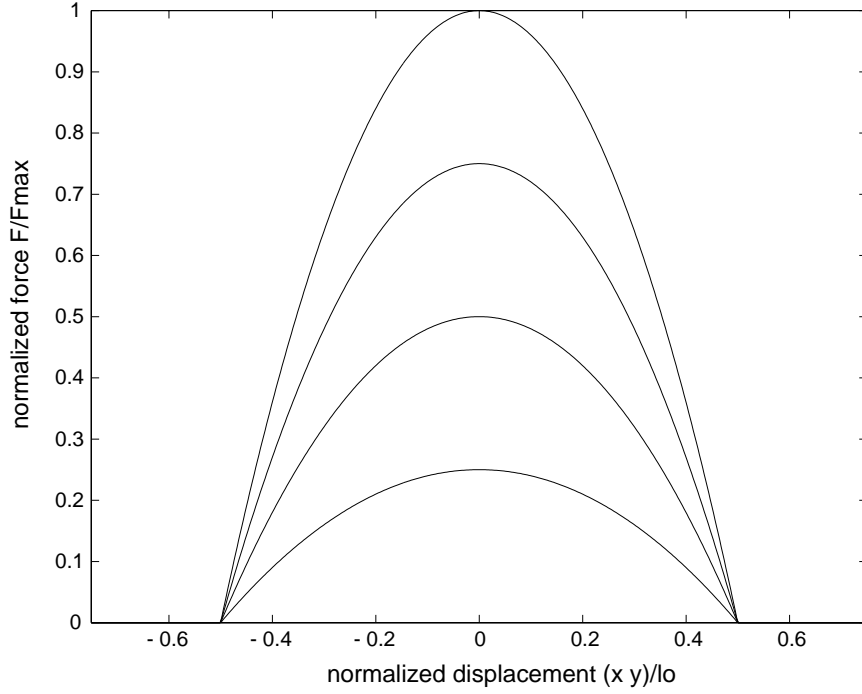


FIGURE 4. The force in the contractile element (CE) is assumed to vary parabolically with displacement and linearly with activation.

where

$$F_{top} = K_{fibers} y = F_{ce} \quad (3)$$

$$F_{bottom} = K_{matrix} x \quad (4)$$

Substituting for F_{ce} and expanding the equation for F_{top} results in a quadratic equation in the internal variable y

$$0 = \frac{4}{l_o^2} F_{max} \alpha y^2 - \left(\frac{8}{l_o^2} F_{max} \alpha x + K_{fibers} \right) y + \frac{4}{l_o^2} F_{max} \alpha \left[x^2 - \left(\frac{l_o}{2} \right)^2 \right] \quad (5)$$

Finally, the desired stress can be calculated as

$$\sigma = \frac{F}{A} = \frac{K_{fibers} y + K_{matrix} x}{A} \quad (6)$$

Figure 5 shows a plot of the constitutive law for the problem of interest. Each curve represents a different level of activation, with the maximum possible force increasing proportional to activation. The lowest curve corresponds to the passive linear stretching of the matrix at $\alpha = 0$. The top curve shows the response of the sarcomere at maximum activation, i.e., $\alpha = 1$. At a displacement of 38% of nominal sarcomere length, the muscle generates a peak force of 1.2 times the peak isometric force F_{max} .

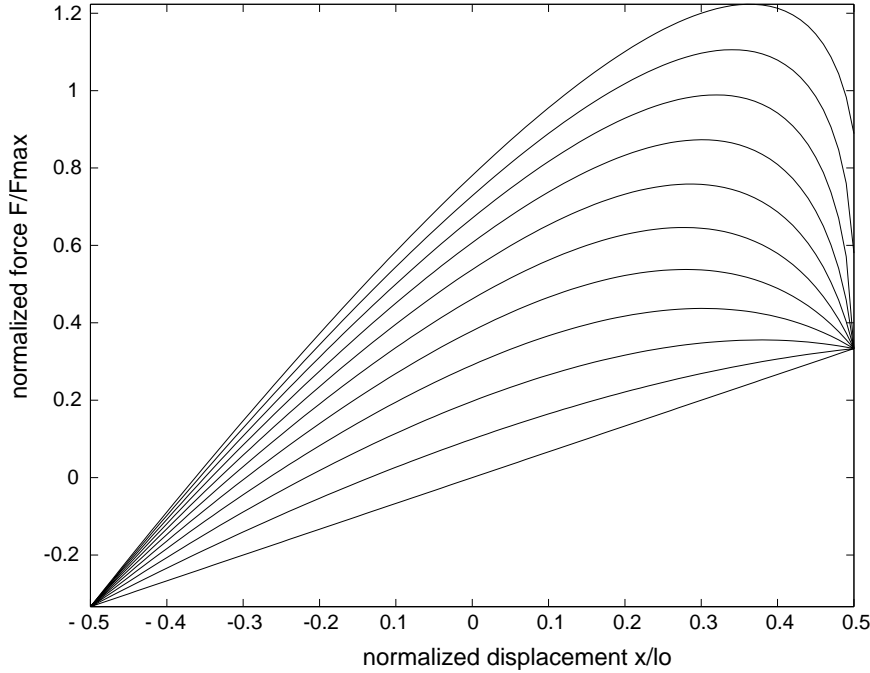


FIGURE 5. The constitutive law for the sarcomere combines the behavior of the contractile element (Fig. 4) with the passive elasticity of the fibers and matrix.

Numerical values for the physical parameters of the model are based on Winters' data (1990). The cross-sectional area of muscle is 20 cm^2 , and its nominal length is 30 cm . The maximum isometric contraction force generated by the muscle is $F_{max} = 800 \text{ N}$ (approximately half of body weight), corresponding to a peak stress of $\sigma_{max} = 0.4 \text{ MPa}$. We used spring constants of $K_{fibers} = 8900 \text{ N/m}$ and $K_{matrix} = 1800 \text{ N/m}$.

2.2 Strong form

For the purposes of this analysis, we select a simple initial-boundary value problem with the unknown displacement field $d(z)$. The muscle is assumed to be quasi-static, thus neglecting acceleration terms. We then express conservation of linear momentum as

$$\frac{\partial \sigma}{\partial z} = 0 \quad 0 < z < L \quad (7)$$

$$\sigma = \sigma(\epsilon, \alpha) \quad \epsilon = \frac{\partial d}{\partial z} \quad \alpha(z) \text{ given} \quad (8)$$

where z is a length coordinate measured along the axis of the one-dimensional muscle and ϵ is the strain. The displacement d of the muscle is defined relative to a zero reference configuration. Dirichlet and Neumann boundary conditions are defined to be

$$d(0) = 0 \quad \sigma(L) \text{ given} \quad (9)$$

Two alternative boundary conditions for the right end $z = L$ are of interest: $d(L)$ given and $\sigma(L) = K_{end} d(L)$ for a stiffness coefficient K_{end} .

2.3 Weak form

Let \mathcal{S} be the space of trial solutions and \mathcal{V} be the correspondence space of weighting functions. The weak form of the problem involves finding the solution $d(z)$ in \mathcal{S} such that all weighting functions $w(z)$ in \mathcal{V} satisfy

$$\int_0^L \frac{\partial w}{\partial z} \sigma dz - w(L) \sigma(L) = 0 \quad (10)$$

For alternate boundary conditions (i.e., $z(L) = 0$), the weighting function must satisfy $w(L) = 0$.

2.4 Galerkin finite element approximation

The Galerkin finite element approximation replaces the spaces \mathcal{S} and \mathcal{V} by approximate spaces \mathcal{S}^h and \mathcal{V}^h . We express weighting functions w^h and trial solutions d^h as a linear combination of shape functions

$$w^h(z) = \sum_A N_A(z) w_A \quad d^h(z) = \sum_B N_B(z) d_B \quad (11)$$

where A and B represent nodal indexes. *** For the purposes of this analysis, we use linear shape functions over each element. On the element $[z_A, z_{A+1}]$, the two shape functions are

$$N_A(z) = \frac{z_{A+1} - z}{h} \quad N_{A+1}(z) = \frac{z - z_A}{h} \quad (12)$$

where the mesh size $h = z_{A+1} - z_A$.

2.5 Matrix problem

Since the nonlinear constitutive law for the contractile element is embedded in the evaluation of σ , we express the matrix problem as the vector equation $\mathbf{F}_{int} = \mathbf{F}_{ext}$. The internal force vector represents the stress state of the sarcomeres while the external force vector arises from the boundary conditions

$$F_{int \ A} = \int_0^L \frac{\partial N_A}{\partial z} \sigma \left(\sum_B \frac{\partial N_B}{\partial z} d_B, \alpha \right) dz \quad (13)$$

$$F_{ext \ A} = N_A(L) \sigma(L) \quad \sigma(L) \text{ given} \quad (14)$$

In the case of the Dirichlet boundary condition $w(L) = 0$, the external force vector $\mathbf{F}_{ext} = \mathbf{0}$.

For numerical efficiency, we use the isoparametric coordinate ξ by mapping the element $[z_A, z_{A+1}]$ onto the interval $[-1, 1]$. We can now define and compute the internal force vector for each element. The total internal force vector \mathbf{F}_{int} is the assembly of the contributions from each element. Since there are two shape functions for each element, the element force vector has dimension 2x1 and is given as

$$\mathbf{F}_{int} = \mathbf{A}_e \begin{bmatrix} F_{int \ 1} \\ F_{int \ 2} \end{bmatrix} \quad (15)$$

where \mathbf{A}_e refers to the assembly of the contributions from each element to the global system (see Hughes, 1987 for details). The components of \mathbf{F}_{int} are

$$F_{int\ i} = \int_0^1 \frac{\partial N_i}{\partial \xi} \frac{\partial \xi}{\partial z} \sigma \left(\frac{\partial N_1}{\partial \xi} \frac{\partial \xi}{\partial z} d_1 + \frac{\partial N_2}{\partial \xi} \frac{\partial \xi}{\partial z} d_2, \alpha \right) \frac{\partial z}{\partial \xi} d\xi \quad i \in \{1, 2\} \quad (16)$$

The consistent tangent matrix \mathbf{J} can be derived from the internal force vector

$$\mathbf{J} = \mathbf{A}_e \begin{bmatrix} \frac{\partial F_{int\ 1}}{\partial d_1} & \frac{\partial F_{int\ 1}}{\partial d_2} \\ \frac{\partial F_{int\ 2}}{\partial d_1} & \frac{\partial F_{int\ 2}}{\partial d_2} \end{bmatrix} \quad (17)$$

where

$$\frac{\partial F_{int\ i}}{\partial d_j} = \int_0^1 \frac{\partial N_i}{\partial \xi} \frac{\partial N_j}{\partial \xi} \left(\frac{\partial \xi}{\partial z} \right)^2 \frac{d\sigma}{dz} \left(\frac{\partial N_1}{\partial \xi} \frac{\partial \xi}{\partial z} d_1 + \frac{\partial N_2}{\partial \xi} \frac{\partial \xi}{\partial z} d_2, \alpha \right) \frac{\partial z}{\partial \xi} d\xi \quad i, j \in \{1, 2\} \quad (18)$$

In order to evaluate the derivative of the stress σ with respect to the displacement x of the right end of the sarcomere model, we compute $\frac{dy}{dx}$ from the variational form of Eq. (5)

$$\frac{8}{l_o^2} F_{max} \alpha y dy - \frac{8}{l_o^2} F_{max} \alpha (x dy + y dx) - K_{fibers} dy + \frac{8}{l_o^2} F_{max} \alpha x dx = 0 \quad (19)$$

$$\frac{dy}{dx} = \frac{\frac{8}{l_o^2} F_{max} \alpha (y - x)}{\frac{8}{l_o^2} F_{max} \alpha (y - x) - K_{fibers}} \quad (20)$$

$$\frac{d\sigma}{dx} = \frac{K_{fibers} \frac{dy}{dx} + K_{matrix}}{A} \quad (21)$$

To numerically solve these integrals, we assume that the activation is piecewise constant in space so that α does not vary over an element. Since the explicit arguments of the integrals vary only with the linear shape functions, we use two point Gauss quadrature to evaluate them. However, the constitutive law for σ involves solving a quadratic equation, thereby introducing square roots. Consequently, perfect integration cannot be expected with any Gauss quadrature rule. Still, the two point rule is sufficiently accurate for the desired application.

2.6 Newton-Raphson iteration

As a result of the nonlinear nature of sarcomere constitutive law, the discretized system of algebraic equations expressing momentum balance is nonlinear. We use the Newton-Raphson method to solve for the unknown displacement vector \mathbf{d} . The objective is to minimize the Euclidean norm of the residual vector \mathbf{R} defined by

$$\mathbf{R} = \mathbf{F}_{ext} - \mathbf{F}_{int} \quad (22)$$

Starting from an initial guess, the algorithm solves for \mathbf{d}^{k+1} using the tangent \mathbf{J}^k of the internal force vector. At iteration k an incremental displacement vector $\Delta \mathbf{d}^k$ is computed, from which we obtain a new estimate \mathbf{d}^{k+1} of the solution

$$\mathbf{J}^k \Delta \mathbf{d}^k = \mathbf{R}^k \quad (23)$$

$$\mathbf{d}^{k+1} = \mathbf{d}^k + \Delta \mathbf{d}^k \quad (24)$$

where the force vectors \mathbf{F}_{int} and \mathbf{F}_{ext} and the tangent matrix \mathbf{J} are given by Eqs. (14), (15), and (17) respectively.

2.7 Boundary conditions

The boundary conditions defined in Eq. (9) for the model problem impose the displacement of the muscle at $z = 0$ and the stress at $z = L$. The natural boundary condition at the right end is explicitly contained in the formulation of the external force vector \mathbf{F}_{ext} in Eq. (14). In order to ensure that the solution satisfies the essential boundary condition at the left end, we condense the matrix system (Hughes, 1987).

2.8 Results

Using the finite element implementation with a Newton-Raphson solver, we solved Eq. (10) for three different sets of boundary conditions. The left end boundary condition $d(0) = 0$ remains the same in each case. To determine the model's effectiveness under a variety of loading situations, we analyzed a variety of right end ($z = L$) boundary conditions: prescribed force (traction), fixed displacement, and a spring-like relationship between force and displacement

$$\sigma(L) = 0.125 \text{ MPa} \quad (25)$$

$$d(L) = 0 \quad (26)$$

$$\sigma(L) = 500 z(L) \text{ MPa} \quad (27)$$

Although the finite element method has only been derived with a traction boundary condition, the other two cases are similar and the details are omitted here.

We have obtained plots of the displacement and stress fields along the length of the muscle for various activation patterns using a 200 element mesh. We analyzed the results for six different activation profiles: three constant along the muscle's length (100%, 50%, and 0%) and three which vary with position (ramp and two parabolic shapes).

2.8.1 Prescribed force

The first boundary condition considered is a prescribed tensile force of 250 N applied to the right end of the muscle. Since we consider a static muscle, force equilibrium implies that the corresponding stress of 0.125 MPa is uniformly experienced along the entire muscle length. The plots of Fig. 6 display this uniform stress distribution. While the stress remains invariant with position and activation, the displacement profile depends on the activation pattern. All of the displacement curves satisfy the fixed left end boundary condition. For uniform full muscle activation, the muscle contracts linearly along its length, with a maximum contraction of 8 cm at the right end. Less activation corresponds to less contraction, until the muscle is fully deactivated and the passive elastic properties cause it to stretch linearly to a peak displacement of 12 cm. The curves for variable activation fields on the right suggest the existence of local contraction regimes of the muscle. In the case of a ramp activation the muscle contracts more at the right end than at the left one. The slope of the displacement curve is positive (local expansion) in the region of low activation and negative (local contraction) where the activation is high. The muscle expands near the deactivated left end in response to the local contraction

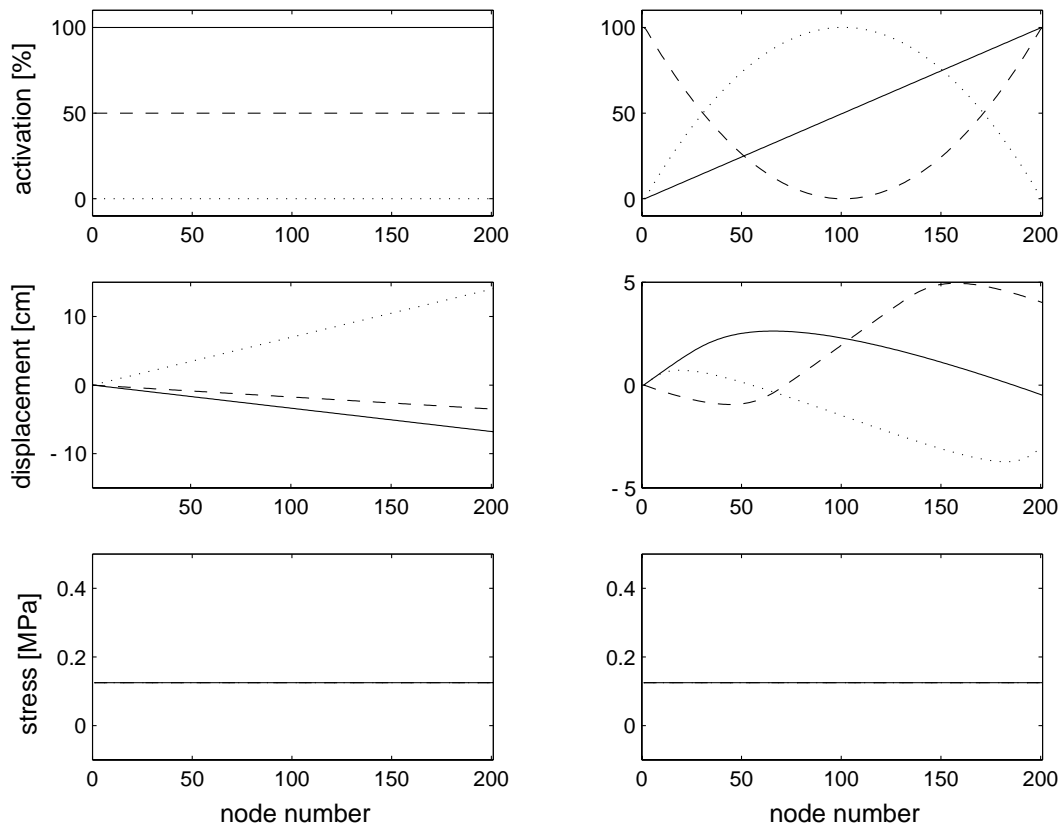


FIGURE 6. Prescribed traction boundary condition with constant (left) and variable (right) activation profiles. Left: —, full activation; ----, half activation; ·····, zero activation. Right: —, ramp activation; ----, edge activation; - - - -, center activation.

regime at the fully activated right end. When the muscle is centrally activated, the displacement slopes downward in the center of the muscle and slopes upward at each end. The local contraction regime in the center pulls on both ends of the muscle. In the case of edge activation, a local contraction regime exists on each end. The resultant displacement at the right end of the model depends on the average activation state of the muscle, which can be determined by the area integral under the activation profile curves. A muscle with higher average activation is found to have more contraction at the right end. Since the edge activation profile has the least area integral of the three variable activation curves, this case corresponds to the least contraction and, in fact, has a positive displacement of 4 cm at the end. On the other hand, center activation results in the largest activation integral and thus the largest contraction.

2.8.2 Fixed displacement

The displacement and stress profiles for an isometric contraction are given in Fig. 7. All of the displacement curves pass through zero at both of the ends of the muscle, corresponding to the Dirichlet boundary conditions. When the muscle

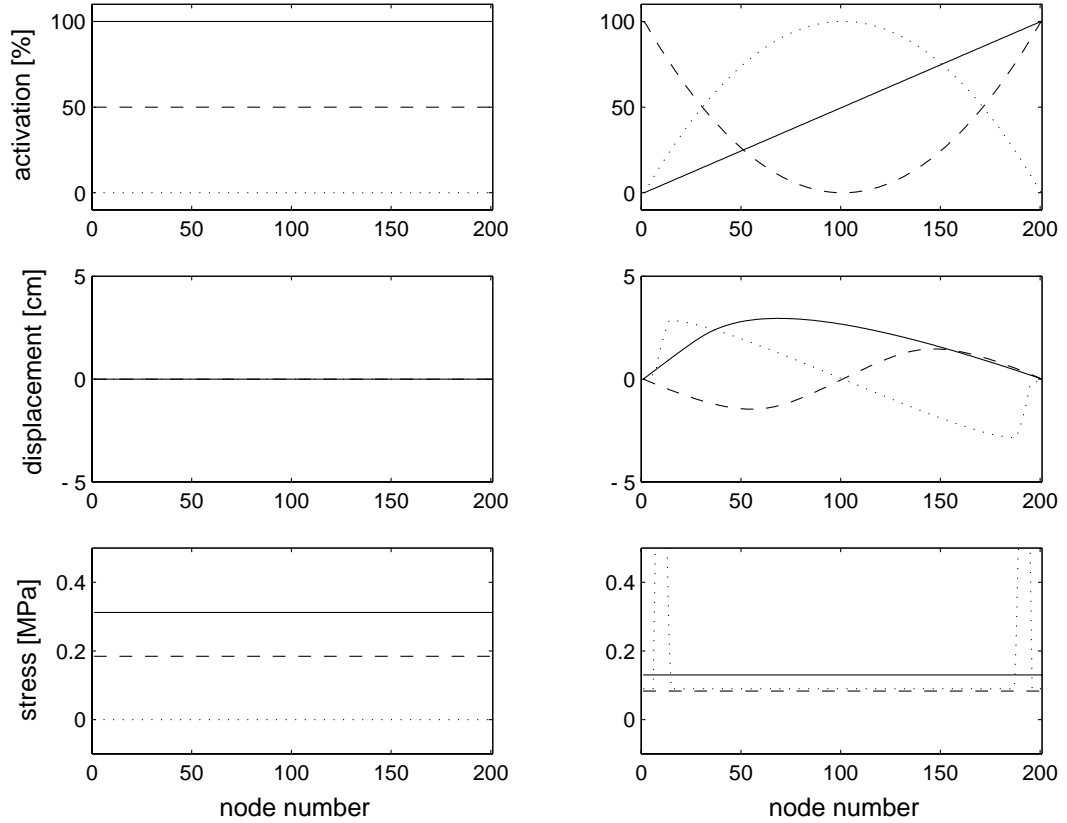


FIGURE 7. Prescribed displacement boundary condition with constant (left) and variable (right) activation profiles. Left: —, full activation; ----, half activation; ·····, zero activation. Right: —, ramp activation; ----, edge activation; ·····, center activation.

experiences uniform activation, there is no local contraction regime, and, consequently, the displacement is zero throughout. However, a nonzero activation causes stress to build up, with a maximum uniform stress of 0.32 MPa for a full (100%) isometric contraction. For the three variable activation profiles, we observe the same local contraction regimes from the slopes of the displacement plots as in Fig. 6, while still satisfying the right end boundary condition. Due to equilibrium considerations, the stress throughout the length of the muscle remains constant. As in Fig. 6, this constant depends on the integral of the activation profile. Hence, a maximum stress occurs for full uniform activation, with decreasing stress for half uniform activation, ramp activation, and edge activation. The results for center activation did not converge and serve as evidence of the numerical difficulties inherent in the implementation of the constitutive model and the Newton-Raphson solving scheme.

2.8.3 Spring-like boundary

A third important boundary condition has a spring of stiffness $K_{end} = 500 \text{ N/m}^3$ attached to the right end of the muscle. This corresponds to the elastic tendon which

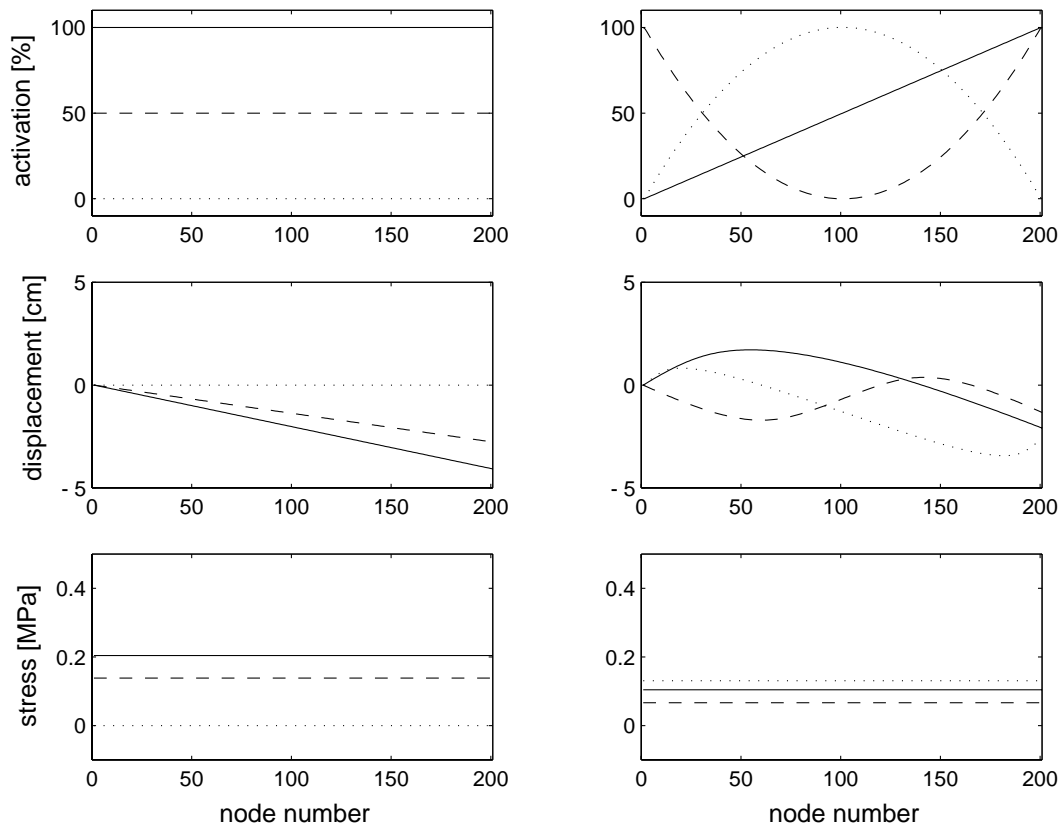


FIGURE 8. Elastic spring boundary condition with constant (left) and variable (right) activation profiles. Left: —, full activation; ----, half activation; ·····, zero activation. Right: —, ramp activation; ----, edge activation; ·····, center activation.

attaches a muscle to the skeleton. The results in Fig. 8 show that all six activation profiles satisfy the specified boundary condition since the stress at the right end is proportional to the magnitude of the displacement through the constant K_{end} . For the three constant activation cases, the displacement varies linearly along the length of the muscle (as in Fig. 6) and the stress is a constant value dependent on the activation level (as in Fig. 7). The displacement profiles for variable activation patterns again exhibit the local contraction regimes of Figs. 6 and 7 but with the right end displacement determined from the stress by the boundary condition. As in Fig. 7, the stress profile is uniform with an amplitude proportional to the integral of the activation curve.

2.9 Discussion

Three boundary conditions have been analyzed, each corresponding to a different loading condition of the muscle. When a force is prescribed at the right end, we determine the constant stress magnitude throughout the muscle's length, but the displacement profile depends on the type of activation. For isometric loading, the displacement of the ends of the muscle remains fixed, but both displacement at

interior points and stress varies with the activation pattern. The third type of boundary, an elastic spring (tendon), combines the behavior of the first two by requiring the displacement and stress at the right end to be proportional.

The stress distribution in every case remains constant along the length of the muscle due to equilibrium. Unless it is specified *a priori*, this stress magnitude is related to the level of activation: a state of higher average activation, as determined by the integral of the activation, causes the muscle to experience greater stress. For example, the stress in the uniform fully activated case always is the largest, followed by the center activated profile.

The dependence of displacement on position obtained in the results underscores the significance of using a continuum approach instead of one lumped parameter element to represent the muscle. When the activation of the muscle is not uniform, neither is the displacement profile. The muscle contracts more in regions of larger activation, called local contraction regimes. In a local contraction regime, the slope of the displacement curve is negative. Conversely, regions of low activation generally have increasing displacement with position. For uniform muscle activation, the displacement interpolates linearly between the displacements at the two boundaries.

In running these simulations, several numerical difficulties, believed to stem from the constitutive model and the use of an exact Newton-Raphson solution scheme, have been encountered (see the center activation case of Fig. 7). In particular, the model only converges under specific choices of the physical parameters. For example, we observed that the stability of the formulation increases with the stiffness K_{matrix} . Still, the issue of numerical convergence and stability remains unresolved.

3. Future plans

The results obtained with the one-dimensional quasi-static muscle model elucidate several features that are captured by a continuum model but not by a one element Hill model. Hill's model assumes that both the muscle's properties and its activation are lumped parameters. In reality, a muscle is far from uniform, especially in cross-sectional area and activation pattern. By employing an approach based on continuum mechanics, the effects of these non-uniformities may be analyzed and better understood.

We will continue work on the one-dimensional model to create a distributed control problem. Future implementations will include additional dynamic effects as modern muscle theory establishes a relationship between muscle force, displacement, and velocity. Since the muscle has mass, inertial effects are necessary. Finally, the activation will vary in time to mimic the temporal control of the muscle by the central nervous system. In order to provide a more physically relevant model problem, the muscle will be considered in context of a musculoskeletal unit such as the elbow joint. In conjunction with implementing the constitutive model, numerical convergence and stability will be addressed. Once we complete the physical model, we will formulate the problem in the context of distributed control by assuming the activation is unknown instead of arbitrarily specified. The ultimate objective is to determine the optimal activation field in space and time that controls the muscle so that it can perform a simple task.

REFERENCES

- HILL, A. V. 1938 The heat of shortening and the dynamic constants of muscle. *Proceedings of the Royal Society, B.* **126**, 136-195.
- HUGHES, THOMAS J. R. 1987 *The Finite Element Method: Linear Static and Dynamic Finite Element Analysis*. Prentice-Hall, Inc.
- HUXLEY, A. F. 1957 Muscle structure and theories of contraction. *Progress in Biophysics and Biophysical Chemistry.* **7**, 257-318.
- WINTERS, JACK M. 1990 Hill-Based Muscle Models: A Systems Engineering Perspective. *Multiple Muscle Systems: Biomechanics and Movement Organization*. J. M. Winters and S. L-Y. Woo, eds., Springer-Verlag. 69-92.
- ZAHALAK, GEORGE I. 1990 Modeling Muscle Mechanics (and Energetics). *Multiple Muscle Systems: Biomechanics and Movement Organization*. J. M. Winters and S. L-Y. Woo, eds., Springer-Verlag. 1-23.
- ZAJAC, FELIX E. & WINTERS, JACK M. 1990 Modeling Musculoskeletal Movement Systems: Joint and Body Segmental Dynamics, Musculoskeletal Actuation and Neuromuscular Control *Multiple Muscle Systems: Biomechanics and Movement Organization*. J. M. Winters and S. L-Y. Woo, eds., Springer-Verlag. 121-148.